

We are IntechOpen, the world's leading publisher of Open Access books Built by scientists, for scientists

6,900

Open access books available

186,000

International authors and editors

200M

Downloads

Our authors are among the

154

Countries delivered to

TOP 1%

most cited scientists

12.2%

Contributors from top 500 universities



WEB OF SCIENCE™

Selection of our books indexed in the Book Citation Index
in Web of Science™ Core Collection (BKCI)

Interested in publishing with us?
Contact book.department@intechopen.com

Numbers displayed above are based on latest data collected.
For more information visit www.intechopen.com



Application of the Continuum-Lattice Thermodynamics

Eun-Suok Oh
University of Ulsan
South Korea

1. Introduction

Through the continuum-lattice thermodynamic approach, the thermodynamic behaviors of two- and three-dimensional multicomponent, elastic, crystalline solids are developed. We begin with a discussion of non-equilibrium thermodynamics of an isolated body that is not undergoing a phase transformation.

Our analysis recognizes that the Helmholtz free energy, \hat{A} , is an explicit function of the deformed crystallographic or lattice vectors defining the deformed crystalline structure. Edelen (1975) gave a similar discussion with the assumption that \hat{A} was an explicit function of the deformation gradient rather than a function of the deformed lattice vectors. For this reason, his analysis requires an additional step in which the implications of the isotropy group are observed (Truesdell & Noll, 1965, p. 310); the requirements of the isotropy group are automatically accounted for in our analysis through the use of the lattice vectors (Slattery & Lagoudas, 2005).

As applications, we obtain the stress-deformation behaviours of graphene, carbon nanotubes (CNTs), boron-nitride nanotubes (BNNTs) which are composed of a regular two-dimensional array of hexagonal lattices of atoms (Oh et al., 2005; Oh, 2010), and the stress-deformation behaviours of face-centred cubic crystals such as diamond, silicon, silicon-carbide, and boron-nitride (Oh & Slattery, 2008). Using an interatomic potential, the Tersoff (Tersoff, 1988; 1989) or Tersoff-like potential (Brenner, 1990; Albe & Moller, 1998; Brenner et al., 2002) to describe interaction between atoms, we compute the elastic properties for the crystals. These are compared with the available experimental and theoretical values.

2. Continuum-lattice thermodynamics

A simple two- or three-dimensional crystal is one in which two or three primitive lattice vectors, vectors drawn between immediate neighbor atoms, can express all of the lattice points as shown in Figs. 1(a) and 1(b) for two-dimensional crystals and in Figs. 2(a) and 2(b) for three-dimensional crystals. Generally, these primitive lattice vectors are not sufficient to describe more complicated structures such as those depicted in Figs. 1(c), 1(d), 2(c), and 2(d). The primitive lattice vectors $\mathbf{e}_{(1)}$ and $\mathbf{e}_{(2)}$ in Fig. 1 and $\mathbf{e}_{(1)}$, $\mathbf{e}_{(2)}$ and $\mathbf{e}_{(3)}$ in Fig. 2—so called external lattice vectors—determine the external structure of the unit cell. In order to describe the internal structure of the unit cell, one or more additional lattice vectors—so called internal lattice vectors—are required, such as $\mathbf{e}_{(3)}$ in Figs. 1(c) and 1(d) or $\mathbf{e}_{(4)}$ in Figs. 2(c) and 2(d).

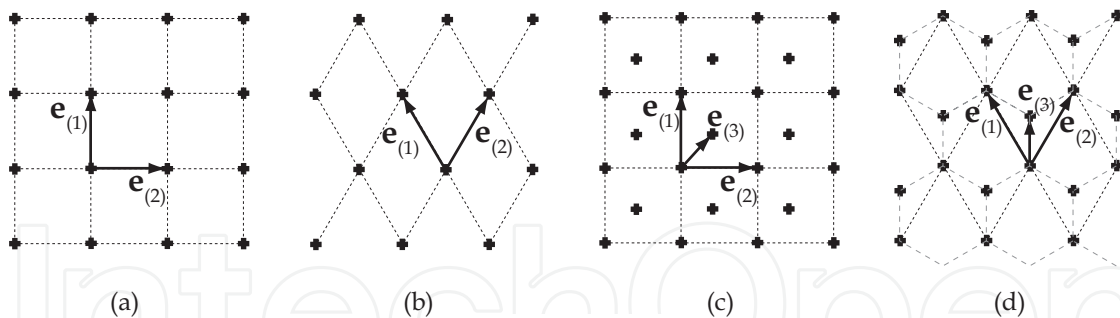


Fig. 1. Two-dimensional lattices: (a) a square Bravais lattice, (b) a diamond Bravais lattice, (c) a more general lattice having a square unit cell, and (d) a hexagonal lattice (Oh et al., 2005).

Our particular interest in what follows is complicated two- or three-dimensional crystals that are not undergoing a phase transformation. As seen in Fig. 3, we will assume that the adjoining phases are not crystalline, and that they are not also undergoing a phase transformation.

For the adjoining non-crystalline phase (gas, liquid, or amorphous solid), we will assume that the Helmholtz free energy per unit mass is given by

$$\hat{A} = \hat{A}(T, \rho, \omega_{(1)}, \dots, \omega_{(N-1)}). \quad (1)$$

Here T is the temperature, ρ is the total mass density, $\omega_{(A)} = \rho_{(A)}/\rho$ is the mass fraction of species A , and $\rho_{(A)}$ is the mass density of species A . For the two- or three-dimensional multicomponent crystal, let us initially assume that the surface Helmholtz free energy per mass is

$$\hat{A} = \hat{A}(T, \rho, \omega_{(1)}, \dots, \omega_{(N-1)}, \mathbf{E}_{(1)}, \dots, \mathbf{E}_{(k)}, \mathbf{e}_{(1)}, \dots, \mathbf{e}_{(k)}). \quad (2)$$

Here $\mathbf{E}_{(i)}$ is a primitive lattice vector in the undeformed configuration and its length will be determined by the equilibrium bond length. Its corresponding lattice vector in the configuration deformed by an in-plane homogeneous deformation, \mathbf{F} , is denoted as $\mathbf{e}_{(i)}$. The deformation gradient is defined as

$$\mathbf{F} \equiv \text{grad } \mathbf{z}, \quad (3)$$

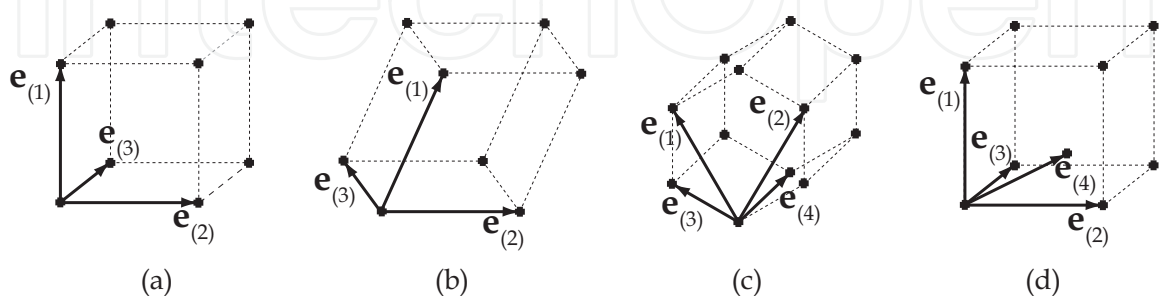


Fig. 2. Three-dimensional lattices: (a) a simple cubic lattice, (b) a rhombohedral lattice, (c) a hexagonal lattice, and (d) a more general cubic lattice having an atom inside unit cell (Oh & Slattery, 2008).

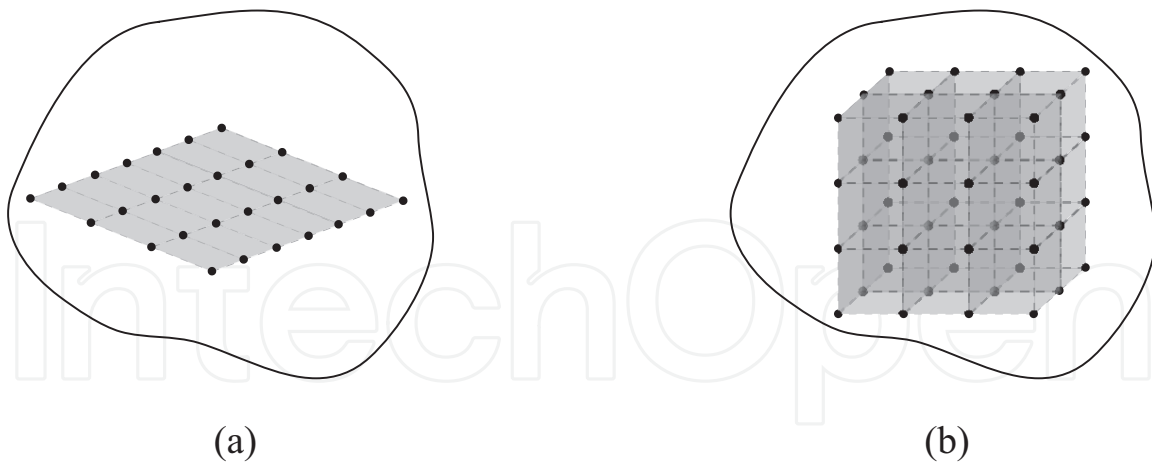


Fig. 3. An isolated body consisting of a crystalline solid and its adjoining phase: (a) two-dimensional crystal and (b) three-dimensional crystal.

where the gradient operation is performed in the undeformed configuration and \mathbf{z} is a position vector. Taking a continuum point of view, we will regard these lattice vectors as being continuous functions of position on the space. Using the Born rule (Ericksen, 1992; Zanzotto, 1992; Klein, 199; James & Hane, 2000; Zhang et al., 2002), we can express the deformed external lattice vectors introduced to describe the external structure of the deformed unit cell as

$$\mathbf{e}_{(i)} \equiv \mathbf{F}\mathbf{E}_{(i)}, \quad i = 1, 2, \text{ for 2-D crystals} \quad \text{or} \quad i = 1, 2, 3 \text{ for 3-D crystals.} \quad (4)$$

It will be shown in equation (40) that the deformed internal lattice vectors $\mathbf{e}_{(i)}$ ($i = 3, \dots, k$ for 2-D crystals or $i = 4, \dots, k$ for 3-D crystals) describing the internal structure of the unit cell are decided by minimizing the Helmholtz free energy at equilibrium.

The principle of frame indifference (Truesdell & Noll, 1965, p. 44) requires that the most general form of such a function is one in which all possible scalar products of the various lattice vectors appear (Truesdell & Noll, 1965, p. 29). We will eliminate scalar products of the form $\mathbf{E}_{(m)} \cdot \mathbf{e}_{(n)}$, since we will show later that they would lead to a non-symmetric stress tensor [see the discussion concluding with equation (38)], which we will not allow in this development. Scalar products of the form $\mathbf{E}_{(m)} \cdot \mathbf{E}_{(n)}$ may be retained in the background contributing to the behaviour of the surface. In view of this reasoning, we will write

$$\hat{A} = \hat{A}(T, \rho, \omega_{(1)}, \dots, \omega_{(N-1)}, \mathbf{e}_{(1)} \cdot \mathbf{e}_{(1)}, \dots, \mathbf{e}_{(1)} \cdot \mathbf{e}_{(k)}, \mathbf{e}_{(2)} \cdot \mathbf{e}_{(2)}, \dots, \mathbf{e}_{(2)} \cdot \mathbf{e}_{(k)}, \mathbf{e}_{(3)} \cdot \mathbf{e}_{(3)}, \dots, \mathbf{e}_{(3)} \cdot \mathbf{e}_{(k)}). \quad (5)$$

Here all other scalar products are excluded from the dependence of \hat{A} since they are not independent variables. It will be more convenient to represent the scalar products appearing in equation (5) as

$$I_{(mn)} \equiv \mathbf{e}_{(m)} \cdot \mathbf{e}_{(n)} - \mathbf{E}_{(m)} \cdot \mathbf{E}_{(n)} \quad m = 1, 2, 3 \text{ and } n = 1, \dots, k, \quad (6)$$

and equation (5) becomes

$$\hat{A} = \hat{A}(T, \rho, \omega_{(1)}, \dots, \omega_{(N-1)}, I_{(11)}, \dots, I_{(1k)}, I_{(22)}, \dots, I_{(2k)}, I_{(33)}, \dots, I_{(3k)}). \quad (7)$$

Using equation (4) and the definition of the right Cauchy–Green strain tensor (Slattery et al., 2007, p. 7):

$$\mathbf{C} \equiv \mathbf{F}^T \mathbf{F} \quad (8)$$

we can express the scalar products in equation (6) for three-dimensional crystals as

$$\begin{aligned} I_{(mn)} &= \mathbf{F}\mathbf{E}_{(m)} \cdot \mathbf{F}\mathbf{E}_{(n)} - \mathbf{E}_{(m)} \cdot \mathbf{E}_{(n)} \\ &= \mathbf{E}_{(m)} \cdot \mathbf{F}^T \mathbf{F} \mathbf{E}_{(n)} - \mathbf{E}_{(m)} \cdot \mathbf{E}_{(n)} \\ &= \mathbf{E}_{(m)} \cdot (\mathbf{C} - \mathbf{I}) \mathbf{E}_{(n)} \quad m, n = 1, 2, 3. \end{aligned} \quad (9)$$

In addition, because the components of \mathbf{C} are constrained by (Slattery, 1999, p. 49)

$$\sqrt{\det \mathbf{C}} = \frac{\rho_\kappa}{\rho}, \quad (10)$$

we see that ρ , $I_{(11)}$, $I_{(12)}$, $I_{(13)}$, $I_{(22)}$, $I_{(23)}$, and $I_{(33)}$ are not independent variables. For these reasons, we will write equation (7) as

$$\hat{A} = \hat{A}(T, \omega_{(1)}, \dots, \omega_{(N-1)}, I_{(11)}, \dots, I_{(1k)}, I_{(22)}, \dots, I_{(2k)}, I_{(33)}, \dots, I_{(3k)}), \quad (11)$$

for three-dimensional crystals.

In a very similar way, the Holmholtz free energy per unit mass for a two-dimensional multicomponent crystal can be expressed as

$$\hat{A} = \hat{A}(T, \omega_{(1)}, \dots, \omega_{(N-1)}, I_{(11)}, I_{(12)}, I_{(22)}, I_{(13)}, \dots, I_{(1k)}, I_{(23)}, \dots, I_{(2k)}). \quad (12)$$

In order to simplify our theoretical approach, we will confine to three-dimensional crystals until we apply the results to some crystalline solids.

2.1 Euler, Gibbs, and Gibbs–Duhem equations

From the differential entropy inequality (Slattery, 1999, p. 438), we conclude

$$\hat{S} = - \left(\frac{\partial \hat{A}}{\partial T} \right)_{\omega_{(A)}, I_{(mn)}} \quad (13)$$

where \hat{S} is the entropy per unit mass. Slattery & Lagoudas (2005) have shown that

$$\left(\frac{\partial \hat{A}}{\partial \omega_{(A)}} \right)_{T, \omega_{(C \neq A)}, I_{(mn)}} = \mu_{(A)} - \mu_{(N)}, \quad (14)$$

where $\mu_{(A)}$ is the chemical potential of species A on a mass basis. We will also let (Slattery & Lagoudas, 2005)

$$\mu_{(I, mn)} \equiv \left(\frac{\partial \hat{A}}{\partial I_{(mn)}} \right)_{T, \omega_{(A)}, I_{(pq \neq mn)}} \quad (15)$$

With these expressions, the differentiation of equation (11) can be expressed as

$$\begin{aligned} d\hat{A} &= -\hat{S}dT + \sum_{A=1}^{N-1} (\mu_{(A)} - \mu_{(N)}) d\omega_{(A)} + \sum_{m=1}^3 \sum_{n=m}^k \mu_{(I,mn)} dI_{(mn)} \\ &= -\hat{S}dT + \sum_{A=1}^N \mu_{(A)} d\omega_{(A)} + \sum_{m=1}^3 \sum_{n=m}^k \mu_{(I,mn)} dI_{(mn)}. \end{aligned} \quad (16)$$

This is referred to as the modified Gibbs equation.

In view of the Euler's equation (Slattery et al., 2007, p. 310)

$$\hat{A} = -\frac{P}{\rho} + \sum_{A=1}^N \mu_{(A)} \omega_{(A)}, \quad (17)$$

where the thermodynamic pressure is defined as (Slattery et al., 2007, p. 309)

$$P \equiv \rho^2 \left(\frac{\partial \hat{A}}{\partial \rho} \right)_{T, \omega_{(A)}}. \quad (18)$$

The modified Gibbs–Duhem equation follows immediately by subtracting equation (16) from the differentiation of equation (17):

$$\hat{S}dT + \frac{P}{\rho^2} d\rho - \frac{dP}{\rho} + \sum_{A=1}^N \omega_{(A)} d\mu_{(A)} - \sum_{m=1}^3 \sum_{n=m}^k \mu_{(I,mn)} dI_{(mn)} = 0. \quad (19)$$

We would like to emphasize that the Euler's equation, the modified Gibbs equation, and the modified Gibbs–Duhem equation all apply to dynamic processes, so long as the underlying assumption about behaviour (11) is applicable.

3. Equilibrium: constraints on isolated systems

We define *equilibrium* to be achieved by an isolated body, when the entropy inequality becomes an equality. In the following sections, we wish to develop necessary and sufficient criteria for the achievement of equilibrium in the isolated body shown in Fig. 4. The following assumptions will be made

1. Once the body is isolated, it is totally enclosed by an impermeable, adiabatic boundary, the velocity of which is zero.
2. There is no mass transfer between the crystalline solid and its adjoining phase in the isolated body
3. No chemical reactions occur.

Let us begin by examining the constraints imposed upon the isolated body by the mass balance, by the momentum balance, by the energy balance, and by the entropy inequality.

3.1 Species mass balance

Since no chemical reactions occur in the isolated body, the mass balance for each species requires (Slattery et al., 2007, p. 269)

$$\frac{d}{dt} \left(\int_R \rho \omega_{(A)} dV \right) = 0. \quad (20)$$

Here dV indicates that a volume integration is to be performed. Applying the transport theorem for a multiphase body (Slattery, 1999, p. 433), we conclude

$$Z_{(A)} \equiv \int_R \left(\rho \frac{d_{(m)}\omega_{(A)}}{dt} \right) dV + \int_{\Sigma} [\rho\omega_{(A)}(\mathbf{v} - \mathbf{u}) \cdot \boldsymbol{\zeta}] dA = 0. \quad (21)$$

Here $d_{(m)}/dt$ is the derivative following a material particle within a phase (Slattery, 1999, p. 4), \mathbf{v} is the mass average velocity, and \mathbf{u} is the time rate of change of position following a surface point (Slattery, 1999, p. 23). The boldface brackets denote the jump quantity enclosed across the interface between phases α and β

$$[\mathbf{S}\boldsymbol{\zeta}] \equiv \mathbf{S}^{(\alpha)}\boldsymbol{\zeta}^{(\alpha)} + \mathbf{S}^{(\beta)}\boldsymbol{\zeta}^{(\beta)}, \quad (22)$$

where $\mathbf{S}^{(\alpha)}$ is the value of the quantity \mathbf{S} in phase α adjacent to the interface Σ and $\boldsymbol{\zeta}^{(\alpha)}$ is the unit normal to the interface pointing into phase α .

3.2 Momentum balance

Since the body is isolated, the sum of the forces exerted upon the body is zero, and the momentum balance requires (Slattery, 1999, p. 33):

$$\begin{aligned} \frac{d}{dt} \left(\int_R \rho \mathbf{v} dV \right) &= \int_S \mathbf{T}\mathbf{n} dA + \int_R \sum_{A=1}^N \rho_{(A)} \mathbf{b}_{(A)} dV \\ &= \int_R \left(\operatorname{div} \mathbf{T} + \sum_{A=1}^N \rho_{(A)} \mathbf{b}_{(A)} \right) dV + \int_{\Sigma} [\mathbf{T}\boldsymbol{\zeta}] dA, \end{aligned} \quad (23)$$

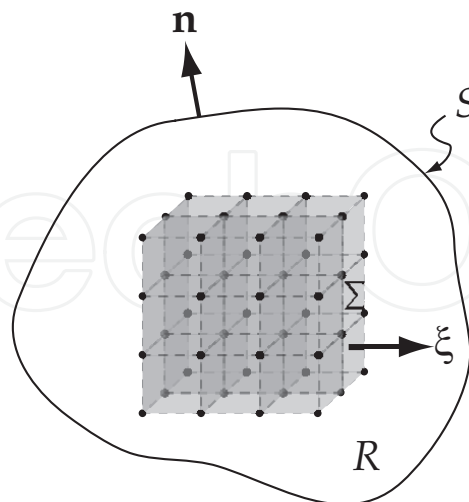


Fig. 4. An isolated body consisting of a three-dimensional crystalline solid and its adjoining phase. R indicates a region occupied by the body, S is a bounding surface of the body, and Σ denote a phase interface between the crystal and its adjoining phase. \mathbf{n} and $\boldsymbol{\zeta}$ are unit normal vectors to the surfaces S and Σ , respectively.

where \mathbf{T} is the Cauchy stress tensor, and $\mathbf{b}_{(A)}$ is the body force per unit mass acting at each point within each phase. Here we have employed the divergence theorem (Slattery, 1999, p. 682). Again applying the transport theorem (Slattery, 1999, p. 433), we see

$$\begin{aligned} \mathbf{Z}_m &\equiv \int_R \left(\rho \frac{d_{(m)}\mathbf{v}}{dt} - \operatorname{div} \mathbf{T} - \sum_{A=1}^N \rho_{(A)} \mathbf{b}_{(A)} \right) dV + \int_{\Sigma} [\rho \mathbf{v}(\mathbf{v} - \mathbf{u}) \cdot \boldsymbol{\xi} - \mathbf{T} \boldsymbol{\xi}] dA \\ &= 0. \end{aligned} \quad (24)$$

3.3 Energy balance

For this isolated body totally enclosed by an adiabatic boundary, the energy balance states that (Slattery et al., 2007, p. 288)

$$\begin{aligned} \frac{d}{dt} \left[\int_R \rho \left(\hat{U} + \frac{v^2}{2} \right) dV \right] &= \int_S \mathbf{v} \cdot \mathbf{T} \mathbf{n} dA + \int_R \mathbf{v} \cdot \sum_{A=1}^N \rho_{(A)} \mathbf{b}_{(A)} dV \\ &= \int_R \left[\mathbf{v} \cdot \left(\operatorname{div} \mathbf{T} + \sum_{A=1}^N \rho_{(A)} \mathbf{b}_{(A)} \right) + \operatorname{tr}(\mathbf{T} \nabla \mathbf{v}) \right] dV + \int_{\Sigma} [\mathbf{v} \cdot \mathbf{T} \boldsymbol{\xi}] dA. \end{aligned} \quad (25)$$

The contact forces do no work, since the boundary of the body is fixed in space. The boundary is adiabatic, which we interpret here as meaning that there is neither contact energy transmission with the surroundings nor external radiant energy transmission. We neglect the possibility of mutual radiant energy transmission. The time rate of change of the internal and kinetic energy of the body is the result only of work done by the body forces. We also neglect the possibility of mutual radiant energy transmission. In the second line we have once again used the transport theorem (Slattery, 1999, p. 433).

We can summarize equation (25) as

$$\begin{aligned} Z_e &\equiv \int_R \left[\rho \frac{d_{(m)} \left(\hat{U} + v^2/2 \right)}{dt} - \mathbf{v} \cdot \left(\operatorname{div} \mathbf{T} + \sum_{A=1}^N \rho_{(A)} \mathbf{b}_{(A)} \right) - \operatorname{tr}(\mathbf{T} \nabla \mathbf{v}) \right. \\ &\quad \left. - \sum_{A=1}^N \rho_{(A)} (\mathbf{v}_{(A)} - \mathbf{v}) \cdot \mathbf{b}_{(A)} \right] dV + \int_{\Sigma} \left[\rho \left(\hat{U} + \frac{v^2}{2} \right) (\mathbf{v} - \mathbf{u}) \cdot \boldsymbol{\xi} - \mathbf{v} \cdot \mathbf{T} \boldsymbol{\xi} \right] dA \\ &= 0. \end{aligned} \quad (26)$$

3.4 Entropy inequality

For the isolated body under consideration here, the entropy inequality says that the time rate of change of the body's entropy must be greater than or equal to zero (Slattery et al., 2007, p. 295):

$$\frac{d}{dt} \left(\int_R \rho \hat{S} dV \right) \geq 0. \quad (27)$$

Equilibrium is achieved, when this inequality becomes an equality. Applying the transport theorem again (Slattery, 1999, p. 433), we find that this may also be written as

$$\int_R \rho \frac{d_{(m)} \hat{S}}{dt} dV + \int_{\Sigma} [\rho \hat{S} (\mathbf{v} - \mathbf{u}) \cdot \boldsymbol{\xi}] dA \geq 0. \quad (28)$$

4. Implications of equilibrium

As explained above, if equilibrium is to be achieved, the left side of equation (27) must be minimized and approaches to zero within the constraints imposed by conservation of mass for each species, by the momentum balance, and by the energy balance as developed in the prior section.

In view of equations (21), (24), and (26), there is no loss in generality in writing equation (28) as (Slattery et al., 2007, p. 391)

$$\int_R \rho \frac{d_{(m)}\hat{S}}{dt} dV + \int_{\Sigma} \left[\rho \hat{S} (\mathbf{v} - \mathbf{u}) \cdot \boldsymbol{\zeta} \right] dA + \sum_{A=1}^N \lambda_{(A)} Z_{(A)} + \boldsymbol{\lambda}_m \cdot \mathbf{Z}_m + \lambda_e Z_e \geq 0, \quad (29)$$

where $\lambda_{(A)}$ and λ_e are constants or Lagrangian multipliers, and $\boldsymbol{\lambda}_m$ is a constant spatial vector, the components of which are Lagrangian multipliers.

From the modified Gibbs equation (16) and the definition of $\hat{A} \equiv \hat{U} - T\hat{S}$ (Slattery et al., 2007, p. 305), we see that

$$\frac{d_{(m)}\hat{S}}{dt} = \frac{1}{T} \frac{d_{(m)}\hat{U}}{dt} - \frac{1}{T} \sum_{A=1}^N \mu_{(A)} \frac{d\omega_{(A)}}{dt} - \frac{1}{T} \sum_{m=1}^3 \sum_{n=m}^k \mu_{(I,mn)} \frac{d_{(m)}I_{(mn)}}{dt}. \quad (30)$$

We will also need from equation (6)

$$\begin{aligned} \frac{d_{(m)}I_{(mn)}}{dt} &= \frac{d_{(m)}\mathbf{e}_{(m)}}{dt} \cdot \mathbf{e}_{(n)} + \mathbf{e}_{(m)} \cdot \frac{d_{(m)}\mathbf{e}_{(n)}}{dt} \\ &= \frac{d_{(m)}\mathbf{F}}{dt} \mathbf{E}_{(m)} \cdot \mathbf{e}_{(n)} + \mathbf{e}_{(m)} \cdot \frac{d_{(m)}\mathbf{F}}{dt} \mathbf{E}_{(n)} \\ &= \nabla \mathbf{v} \mathbf{e}_{(m)} \cdot \mathbf{e}_{(n)} + \mathbf{e}_{(m)} \cdot \nabla \mathbf{v} \mathbf{e}_{(n)} \\ &= \text{tr} \left[\left(\mathbf{e}_{(m)} \otimes \mathbf{e}_{(n)} + \mathbf{e}_{(n)} \otimes \mathbf{e}_{(m)} \right) \nabla \mathbf{v}^T \right] \quad m, n = 1, 2, 3. \end{aligned} \quad (31)$$

Here we used

$$\frac{d_{(m)}\mathbf{F}}{dt} = (\nabla \mathbf{v}) \mathbf{F}, \quad (32)$$

and $\mathbf{e}_{(i)} \otimes \mathbf{e}_{(j)}$ is the tensor product or dyadic product of two vectors $\mathbf{e}_{(i)}$ and $\mathbf{e}_{(j)}$. After rearranging equation (29) by means of equations (21) through (31), we have

$$\begin{aligned} &\int_R \left\{ \rho \left(\frac{1}{T} + \lambda_e \right) \frac{d_{(m)}\hat{U}}{dt} + \sum_{A=1}^N \rho \left(-\frac{\mu_{(A)}}{T} + \lambda_{(A)} \right) \frac{d\omega_{(A)}}{dt} \right. \\ &\quad \left. - \sum_{A=1}^N \rho_{(A)} \lambda_e (\mathbf{v}_{(A)} - \mathbf{v}) \cdot \mathbf{b}_{(A)} - \frac{\rho}{T} \sum_{m=1}^3 \sum_{n=4}^k \mu_{(I,mn)} \frac{d_{(m)}I_{(mn)}}{dt} \right. \\ &\quad \left. - \frac{1}{T} \text{tr} \left[\left(T \lambda_e \mathbf{T} + \rho \sum_{m=1}^3 \sum_{n=m}^3 \mu_{(I,mn)} (\mathbf{e}_{(m)} \otimes \mathbf{e}_{(n)} + \mathbf{e}_{(n)} \otimes \mathbf{e}_{(m)}) \right) \nabla \mathbf{v}^T \right] \right\} dV \\ &+ \int_{\Sigma} \left[\rho \left\{ \left(\frac{1}{T} + \lambda_e \right) \hat{U} + \frac{P}{T\rho} - \sum_{A=1}^N \left(\frac{\mu_{(A)}\omega_{(A)}}{T} - \lambda_{(A)}\omega_{(A)} \right) - \frac{\lambda_e}{2} v^2 \right\} (\mathbf{v} - \mathbf{u}) \cdot \boldsymbol{\zeta} \right. \\ &\quad \left. + \rho (\boldsymbol{\lambda}_m + \lambda_e \mathbf{v}) \cdot [\mathbf{v} \otimes (\mathbf{v} - \mathbf{u}) - \mathbf{T}] \boldsymbol{\zeta} \right] dA \\ &\geq 0. \end{aligned} \quad (33)$$

In arriving at this result, we have recognized the differential momentum balance (Slattery, 1999, p. 434).

Necessary and sufficient conditions for equation (33) to be satisfied in the presence of small perturbations to the system are

$$T = -\frac{1}{\lambda_e} = \text{a constant}, \quad (34)$$

$$\mu_{(A)} = T\lambda_{(A)} \quad \text{for each species } A = 1, 2, \dots, N, \quad (35)$$

$$\mathbf{v}_{(A)} = \mathbf{v} \quad \text{for each species } A = 1, 2, \dots, N, \quad (36)$$

$$\mu_{(I,mn)} = 0 \quad \text{for } m = 1, 2, 3 \text{ and } n = 4, \dots, k, \quad (37)$$

$$\mathbf{T} = \rho \sum_{m=1}^3 \sum_{n=m}^3 \mu_{(I,mn)} \left(\mathbf{e}_{(m)} \otimes \mathbf{e}_{(n)} + \mathbf{e}_{(n)} \otimes \mathbf{e}_{(m)} \right), \quad (38)$$

and

$$\text{on } \Sigma: \quad \mathbf{v} = \mathbf{u} = T\lambda_m. \quad (39)$$

It is important to recognize that equation (38) is the description of stress-deformation behaviour of three-dimensional elastic crystalline solids. From equations (15) and (37), we can express that

$$\left(\frac{\partial \hat{A}}{\partial I_{(mn)}} \right)_{T, \omega_{(A)}, I_{(pq \neq mn)}} = 0 \quad m = 1, 2, 3 \text{ and } n = 4, \dots, k. \quad (40)$$

These relations determine $\mathbf{e}_{(4)}, \dots, \mathbf{e}_{(k)}$ at equilibrium. Notice that, if we had retained scalar products of the form $\mathbf{E}_{(m)} \cdot \mathbf{e}_{(n)}$ in equation (5), the stress tensor would have been non-symmetric.

For a two-dimensional crystalline solid, similar results can be obtained (Oh et al., 2005) as follows:

$$\mathbf{T}^{(\sigma)} = \rho^{(\sigma)} \sum_{m=1}^2 \sum_{n=m}^2 \mu_{(I,mn)} \left(\mathbf{e}_{(m)} \otimes \mathbf{e}_{(n)} + \mathbf{e}_{(n)} \otimes \mathbf{e}_{(m)} \right), \quad (41)$$

and

$$\left(\frac{\partial \hat{A}}{\partial I_{(mn)}} \right)_{T, \omega_{(A)}, I_{(pq \neq mn)}} = 0 \quad m = 1, 2 \text{ and } n = 3, \dots, k. \quad (42)$$

Here the superscript (σ) denotes values assigned to a phase interphase.

5. Stress-deformation behaviour at equilibrium in the limit of infinitesimal deformations

Since it is common to consider infinitesimal deformations, let us consider how equation (38) reduces in this limit:

$$\begin{aligned} \mathbf{T} &= \rho \sum_{m=1}^3 \sum_{n=m}^3 \mu_{(I,mn)} \left(\mathbf{e}_{(m)} \otimes \mathbf{e}_{(n)} + \mathbf{e}_{(n)} \otimes \mathbf{e}_{(m)} \right) \\ &= \rho \sum_{m=1}^3 \sum_{n=m}^3 \mu_{(I,mn)} \left(\mathbf{F}\mathbf{E}_{(m)} \otimes \mathbf{F}\mathbf{E}_{(n)} + \mathbf{F}\mathbf{E}_{(n)} \otimes \mathbf{F}\mathbf{E}_{(m)} \right) \\ &= \rho \sum_{m=1}^3 \sum_{n=m}^3 \mu_{(I,mn)} \mathbf{F} \left(\mathbf{E}_{(m)} \otimes \mathbf{E}_{(n)} + \mathbf{E}_{(n)} \otimes \mathbf{E}_{(m)} \right) \mathbf{F}^T. \end{aligned} \quad (43)$$

Define

$$\mathbf{w} \equiv \mathbf{z} - \mathbf{z}_\kappa, \quad (44)$$

to be the displacement vector, and \mathbf{z} and \mathbf{z}_κ are the position vectors of a material particle in the deformed and undeformed configurations. It follows that the *displacement gradient* is

$$\mathbf{H} \equiv \text{grad } \mathbf{w} = \mathbf{F} - \mathbf{I}. \quad (45)$$

Let ϵ be a very small dimensionless variable characterizing an infinitesimal deformation process. We will seek a solution of the form

$$\mathbf{w} = \mathbf{w}_{(0)} + \epsilon \mathbf{w}_{(1)} + \epsilon^2 \mathbf{w}_{(2)} + \dots. \quad (46)$$

Let us recognize that in the absence of an infinitesimal deformation or as $\epsilon \rightarrow 0$

$$\mathbf{w}_{(0)} = 0. \quad (47)$$

This means that

$$\mathbf{H} = \epsilon \mathbf{H}_{(1)} + \epsilon^2 \mathbf{H}_{(2)} + \dots, \quad \text{where } \mathbf{H}_{(i)} = \text{grad } \mathbf{w}_{(i)}, \quad (48)$$

and thus the right Cauchy-Green strain tensor becomes

$$\begin{aligned} \mathbf{C} &\equiv \mathbf{F}^T \mathbf{F} \\ &= (\mathbf{I} + \epsilon \mathbf{H}_{(1)} + \dots)^T (\mathbf{I} + \epsilon \mathbf{H}_{(1)} + \dots) \\ &= \mathbf{I} + \epsilon (\mathbf{H}_{(1)} + \mathbf{H}_{(1)}^T) + O(\epsilon^2). \end{aligned} \quad (49)$$

From (10) and (49), we find that

$$\begin{aligned} \rho &= \frac{\rho_\kappa}{\sqrt{\det \mathbf{C}}} \\ &= \frac{\rho_\kappa}{\sqrt{\det [\mathbf{I} + \epsilon (\mathbf{H}_{(1)} + \mathbf{H}_{(1)}^T)]} + \dots} \\ &= \frac{\rho_\kappa}{\det \mathbf{I}} - \epsilon \frac{\rho_\kappa}{2(\det \mathbf{I})^2} \text{tr} (\mathbf{H}_{(1)} + \mathbf{H}_{(1)}^T) + \dots \\ &= \rho_\kappa - \epsilon \frac{\rho_\kappa}{2} \text{tr} (\mathbf{H}_{(1)} + \mathbf{H}_{(1)}^T) + \dots. \end{aligned} \quad (50)$$

Since, in the limit of small deformations, the strain

$$\begin{aligned} \boldsymbol{\epsilon} &\equiv \frac{1}{2} [\text{grad } \mathbf{w} + (\text{grad } \mathbf{w})^T] = \epsilon \frac{1}{2} (\mathbf{H}_{(1)} + \mathbf{H}_{(1)}^T) + \dots \\ &= \epsilon \boldsymbol{\epsilon}_{(1)} + \dots, \end{aligned} \quad (51)$$

which allows us to also express equation (50) as

$$\rho = \rho_\kappa (1 - \epsilon \text{tr} \boldsymbol{\epsilon}_{(1)}) + \dots. \quad (52)$$

Equations (45), (48), and (52) also permit us to rewrite equation (43) to the first order in ϵ as (for the moment not addressing the order of $\mu_{(I,mn)}$)

$$\begin{aligned} \mathbf{T} &= \rho_\kappa \left(1 - \epsilon \operatorname{tr} \boldsymbol{\epsilon}_{(1)}\right) \sum_{m=1}^3 \sum_{n=m}^3 \mu_{(I,mn)} \left(\mathbf{I} + \epsilon \mathbf{H}_{(1)}\right) \left(\mathbf{E}_{(m)} \otimes \mathbf{E}_{(n)} + \mathbf{E}_{(n)} \otimes \mathbf{E}_{(m)}\right) \left(\mathbf{I} + \epsilon \mathbf{H}_{(1)}\right)^T \\ &= \rho_\kappa \left(1 - \epsilon \operatorname{tr} \boldsymbol{\epsilon}_{(1)}\right) \sum_{m=1}^3 \sum_{n=m}^3 \mu_{(I,mn)} \left(\mathbf{E}_{(m)} \otimes \mathbf{E}_{(n)} + \mathbf{E}_{(n)} \otimes \mathbf{E}_{(m)}\right) + \rho_\kappa \epsilon \sum_{m=1}^3 \sum_{n=m}^3 \mu_{(I,mm)} \\ &\quad \times \left\{ \mathbf{H}_{(1)} \left(\mathbf{E}_{(m)} \otimes \mathbf{E}_{(n)} + \mathbf{E}_{(n)} \otimes \mathbf{E}_{(m)}\right) + \left[\mathbf{H}_{(1)} \left(\mathbf{E}_{(m)} \otimes \mathbf{E}_{(n)} + \mathbf{E}_{(n)} \otimes \mathbf{E}_{(m)}\right) \right]^T \right\}. \end{aligned} \quad (53)$$

If the reference(or undeformed) configuration is a stress-free configuration,

$$0 = \rho_\kappa \sum_{m=1}^3 \sum_{n=m}^3 \mu_{(I,mn)0} \left(\mathbf{E}_{(m)} \otimes \mathbf{E}_{(n)} + \mathbf{E}_{(n)} \otimes \mathbf{E}_{(m)}\right), \quad (54)$$

where the $\mu_{(I,mn)0}$ are evaluated in the reference configuration. This allows us to write equation (53) as

$$\begin{aligned} \mathbf{T} &= \rho_\kappa \sum_{m=1}^3 \sum_{n=m}^3 \left(\mu_{(I,mn)} - \mu_{(I,mn)0}\right) \left(\mathbf{E}_{(m)} \otimes \mathbf{E}_{(n)} + \mathbf{E}_{(n)} \otimes \mathbf{E}_{(m)}\right) \\ &\quad - \rho_\kappa \epsilon \operatorname{tr} \boldsymbol{\epsilon}_{(1)} \sum_{m=1}^3 \sum_{n=m}^3 \mu_{(I,mn)} \left(\mathbf{E}_{(m)} \otimes \mathbf{E}_{(n)} + \mathbf{E}_{(n)} \otimes \mathbf{E}_{(m)}\right) \\ &\quad + \rho_\kappa \epsilon \sum_{m=1}^3 \sum_{n=m}^3 \mu_{(I,mn)} \left\{ \mathbf{H}_{(1)} \left(\mathbf{E}_{(m)} \otimes \mathbf{E}_{(n)} + \mathbf{E}_{(n)} \otimes \mathbf{E}_{(m)}\right) \right. \\ &\quad \left. + \left[\mathbf{H}_{(1)} \left(\mathbf{E}_{(m)} \otimes \mathbf{E}_{(n)} + \mathbf{E}_{(n)} \otimes \mathbf{E}_{(m)}\right) \right]^T \right\}. \end{aligned} \quad (55)$$

5.1 Implication of a quadratic equation of state

As a special case, let us assume that \hat{A} can be represented as a quadratic function of $I_{(11)}$, $I_{(12)}$, $I_{(12)}$, $I_{(13)}$, $I_{(22)}$, $I_{(23)}$, and $I_{(33)}$ (Truesdell & Noll, 1965, pp. 311-312):

$$\hat{A} = a_{(0)} + \sum_{i=1}^3 \sum_{j=i}^3 a_{(ij)} I_{(ij)} + \frac{1}{2} \sum_{i=1}^3 \sum_{j=i}^3 \sum_{m=1}^3 \sum_{n=m}^3 a_{(ijmn)} I_{(ij)} I_{(mn)} + \dots \quad (56)$$

It should be understood here that $a_{(0)}$, $a_{(ij)}$, and $a_{(ijmn)}$ are functions of temperature and composition with the additional restrictions

$$\begin{aligned} a_{(ij)} &= a_{(ji)} \\ &= \left. \frac{\partial \hat{A}}{\partial I_{(ij)}} \right|_{I_{(pq)}=0}, \end{aligned} \quad (57)$$

and

$$\begin{aligned} a_{(ijmn)} &= a_{(mnij)} \\ &= \left. \frac{\partial^2 \hat{A}}{\partial I_{(ij)} \partial I_{(mn)}} \right|_{I_{(pq)}=0}. \end{aligned} \quad (58)$$

For this special case, from equation (15)

$$\mu_{(I,mn)} = a_{(mn)} + \sum_{i=1}^3 \sum_{j=i}^3 a_{(mnij)} I_{(ij)}, \quad (59)$$

and

$$\mu_{(I,mn)} - \mu_{(I,mn)0} = \sum_{i=1}^3 \sum_{j=i}^3 a_{(mnij)} I_{(ij)}. \quad (60)$$

From equations (9), (49), and (51), we see that

$$\begin{aligned} I_{(ij)} &= \mathbf{E}_{(i)} \cdot (\mathbf{C} - \mathbf{I}) \mathbf{E}_{(j)} \\ &= 2\epsilon \mathbf{E}_{(i)} \cdot \boldsymbol{\epsilon}_{(1)} \mathbf{E}_{(j)}. \end{aligned} \quad (61)$$

To the first order in ϵ , we find that equation (55) reduces to

$$\begin{aligned} \mathbf{T} &= 2\rho\kappa\epsilon \sum_{m=1}^3 \sum_{n=m}^3 \sum_{i=1}^3 \sum_{j=i}^3 \left[a_{(ijmn)} \mathbf{E}_{(i)} \cdot \boldsymbol{\epsilon}_{(1)} \mathbf{E}_{(j)} (\mathbf{E}_{(m)} \otimes \mathbf{E}_{(n)} + \mathbf{E}_{(n)} \otimes \mathbf{E}_{(m)}) \right] \\ &\quad - \rho\kappa\epsilon \operatorname{tr} \boldsymbol{\epsilon}_{(1)} \sum_{m=1}^3 \sum_{n=m}^3 a_{(mn)} (\mathbf{E}_{(m)} \otimes \mathbf{E}_{(n)} + \mathbf{E}_{(n)} \otimes \mathbf{E}_{(m)}) \\ &\quad + \rho\kappa\epsilon \sum_{m=1}^3 \sum_{n=m}^3 a_{(mn)} \left\{ \mathbf{H}_{(1)} (\mathbf{E}_{(m)} \otimes \mathbf{E}_{(n)} + \mathbf{E}_{(n)} \otimes \mathbf{E}_{(m)}) \right. \\ &\quad \left. + \left[\mathbf{H}_{(1)} (\mathbf{E}_{(m)} \otimes \mathbf{E}_{(n)} + \mathbf{E}_{(n)} \otimes \mathbf{E}_{(m)}) \right]^T \right\}. \end{aligned} \quad (62)$$

Using equations (54) and (59), we see that

$$a_{(mn)} = 0. \quad (63)$$

From this, equation (62) reduces to

$$\mathbf{T} = 2\rho\kappa\epsilon \sum_{m=1}^3 \sum_{n=m}^3 \sum_{i=1}^3 \sum_{j=i}^3 a_{(ijmn)} \mathbf{E}_{(i)} \cdot \boldsymbol{\epsilon}_{(1)} \mathbf{E}_{(j)} (\mathbf{E}_{(m)} \otimes \mathbf{E}_{(n)} + \mathbf{E}_{(n)} \otimes \mathbf{E}_{(m)}). \quad (64)$$

5.2 The helmholtz free energy

The internal energy is composed of the kinetic energy associated with molecular motions (translation, rotation, vibration) and the potential energy associated with intermolecular potentials between atoms or molecules (Tester & Modell, 1996, p. 33). Since the molecular kinetic energy is a constant for an isothermal system, the internal energy takes the form

$$\hat{U} = \hat{\Phi} + \text{constant}, \quad (65)$$

where $\hat{\Phi}$ is the intermolecular potential energy.

Since $\hat{A} = \hat{U} - T\hat{S}$ and at equilibrium no changes in temperature or entropy occur, the specific Helmholtz free energy can be written as

$$\hat{A} = \hat{\Phi} + \text{constant}. \quad (66)$$

This represents the relationship between the Helmholtz free energy and the intermolecular potential energy at equilibrium.

We will employ two types of potentials, Tersoff (1988; 1989) and modified Tersoff potentials (Brenner, 1990; Albe & Moller, 1998; Brenner et al., 2002), to describe the interatomic potentials for the crystalline solids. However, the choice of the interatomic potential is rather arbitrary and is dependent of atoms consisting of the crystals.

5.2.1 Tersoff potential

The Tersoff (1988; 1989) potential between atoms i and j separated by the distance, r_{ij} , has the form

$$\Phi_{ij} = f_c(r_{ij})[\Phi_R(r_{ij}) + b_{ij}(r_{ik}, \theta_{ijk}) \Phi_A(r_{ij})], \quad (67)$$

where θ_{ijk} is the angle between bonds $i-j$ and $i-k$ ($k \neq j$). The functions Φ_R , Φ_A , and b_{ij} represent repulsive and attractive pair potentials, and a multi-body coupling between bonds $i-j$ and $i-k$:

$$\begin{aligned} \Phi_R(r) &= A \exp(-\lambda r), \\ \Phi_A(r) &= -B \exp(-\mu r), \end{aligned} \quad (68)$$

and

$$\begin{aligned} b_{ij} &= \chi \left\{ 1 + \beta^n \left[\sum_{k \neq i, j} f_c(r_{ik}) g(\theta_{ijk}) \omega_{ijk} \right]^n \right\}^{-1/2n} \\ g(\theta_{ijk}) &= 1 + \frac{c^2}{d^2} - \frac{c^2}{d^2 + (h - \cos \theta_{ijk})^2}. \end{aligned} \quad (69)$$

The cutoff function is given by

$$f_c(r_{ij}) = \begin{cases} 1, & r < R_1, \\ \frac{1}{2} + \frac{1}{2} \cos \left[\frac{\pi(r - R_1)}{R_2 - R_1} \right], & R_1 \leq r \leq R_2, \\ 0, & r > R_2. \end{cases} \quad (70)$$

Tersoff (1988; 1989) has obtained the sets of parameters for diamond and silicon in Table 1 to fit data given by Yin & Cohen (1983a;b). The sets of the Tersoff potential parameters for boron and nitrogen have been reported by Matsunaga et al. (2000) and Kroll (1996), respectively.

Tersoff (1989) also proposed that the parameters for multicomponent systems such as silicon carbide could be estimated using the following rules:

$$\begin{aligned} A_{\text{Si-C}} &= \sqrt{A_{\text{Si}} A_{\text{C}}}, \quad B_{\text{Si-C}} = \sqrt{B_{\text{Si}} B_{\text{C}}}, \quad \lambda_{\text{Si-C}} = \frac{\lambda_{\text{Si}} + \lambda_{\text{C}}}{2}, \\ \mu_{\text{Si-C}} &= \frac{\mu_{\text{Si}} + \mu_{\text{C}}}{2}, \quad R_{1,\text{Si-C}} = \sqrt{R_{1,\text{Si}} R_{1,\text{C}}}, \quad R_{2,\text{Si-C}} = \sqrt{R_{2,\text{Si}} R_{2,\text{C}}}. \end{aligned} \quad (71)$$

The coefficients in b_{ij} for the multicomponent systems were chosen by the atom corresponding to the first index i . The fitting parameter χ and the C–Si bond length for silicon carbide were $d_0 = 0.9776$ and 1.87 \AA , respectively. For boron nitride, Matsunaga et al. (2000) used $\chi = 1.1593$ and $d_0 = 1.584 \text{ \AA}$. The C–C bond length in diamond and the Si–Si bond length in silicon were 1.54 \AA and 2.35 \AA , respectively.

Parameters	Diamond	Silicon	Boron ^a	Nitrogen ^b
A (eV)	1393.6	1830.8	277.02	11000
B (eV)	346.7	471.2	83.49	219.45
λ (\AA^{-1})	3.4879	2.4799	1.9922	5.7708
μ (\AA^{-1})	2.2119	1.7322	1.5859	2.5115
β (10^{-7})	1.5724	11.0	16.00	1056200
n	0.72751	0.78734	3.9929	12.4498
c	38049	100390	0.52629	79934
d	4.384	16.217	0.001587	134.32
h	-0.57058	-0.59825	0.5	-0.9973
R_1 (\AA)	1.8	2.7	1.8	2.0
R_2 (\AA)	2.1	3.0	2.1	2.3
χ	1	1	1	1
ω_{ijk}	1	1	1	1

^aparameters proposed by Matsunaga et al. (2000)

^bparameters proposed by Kroll (1996)

Table 1. Tersoff potential parameters for C-C in diamond, Si-Si in silicon, B-B in boron, and N-N in nitrogen.

5.2.2 Modified tersoff potentials

A Tersoff-like potential proposed by Brenner (1990) has the same form as the Tersoff potential, except for repulsive and attractive pair potentials:

$$\begin{aligned}\Phi_R(r) &= \frac{D_0}{S-1} \exp \left[-\tau \sqrt{2S} (r - r_0) \right], \\ \Phi_A(r) &= -\frac{SD_0}{S-1} \exp \left[-\tau \sqrt{2/S} (r - r_0) \right],\end{aligned}\tag{72}$$

where D_0 and r_0 are the dimer energy and separation, respectively. The multi-body coupling function has been slightly changed to

$$\begin{aligned}b_{ij} &= \left[1 + \sum_{k \neq i,j} f_c(r_{ik}) g(\theta_{ijk}) \right]^{-\delta}, \\ g(\theta_{ijk}) &= a \left[1 + \frac{c^2}{d^2} - \frac{c^2}{d^2 + (1 + \cos \theta_{ijk})^2} \right].\end{aligned}\tag{73}$$

This potential was employed to describe the interatomic interaction in CNTs and BNNTs including their plane sheets (Oh et al., 2005; Oh, 2010). Some of the potential parameters were adjusted from the original ones provided by Brenner (1990) to fit well the bond length and the cohesive energy of a boron nitride (BN) sheet given in the literature (Moon & Hwang, 2004; Verma et al., 2007). These are listed in Table 2.

Parameters	B. for C-C ^c	T.-B. for B-N ^d	T.-A. ^e for B-N
D_0 (eV)	10953.544	6.36	6.36
S	-	1.0769	1.0769
τ (\AA^{-1})	4.747	2.20	2.0431
r_0 (\AA)	0.313	1.33	1.33
β (10^{-6})	-	-	11.134
δ	0.5	0.382	-
n	-	-	0.36415
a (10^{-4})	2.0813	2.0813	-
c	330	330	1092.93
d	3.5	3.5	12.38
h	-	-	-0.5413
λ_3	-	-	1.9925
ω	1	1	-
R_1 (\AA)	1.7	1.9	1.9
R_2 (\AA)	2.0	2.1	2.1

^cparameters proposed by Brenner et al. (2002)

^dparameters proposed by Oh (2010)

^eparameters proposed by Albe & Moller (1998)

Table 2. Tersoff-like potential parameters for the interaction between atoms.

Albe & Moller (1998) proposed another Tersoff-like potential whose repulsive and attractive pair potentials are the same as (72). The parameter, ω_{ijk} , in the multi-body coupling function (69) was expressed as

$$\omega_{ijk} = \exp [\lambda_3^3 (r_{ij} - r_{ik})^3]. \quad (74)$$

Their potential parameters for boron-nitrogen interactions are also listed in Table 2. Using this potential, Koga et al. (2001) have determined the bond lengths for a cubic BN to be 1.555 \AA . More recently, Brenner et al. (2002) proposed a similar potential to the Tersoff-Brenner potential with new repulsive and attractive pair potentials:

$$\begin{aligned} \Phi_R(r) &= (1 + r_0/r)D_0 e^{-\tau r} f_c(r), \\ \Phi_A(r) &= \sum_{n=1}^3 B_n e^{-\beta_n r}, \end{aligned} \quad (75)$$

where

$$\begin{aligned} B_1 &= 12388.791 \text{ eV}, \quad B_2 = 17.567 \text{ eV}, \quad B_3 = 30.715 \text{ eV}, \\ \beta_1 &= 4.720 \text{ \AA}^{-1}, \quad \beta_2 = 1.433 \text{ \AA}^{-1}, \quad \beta_3 = 1.383 \text{ \AA}^{-1}. \end{aligned} \quad (76)$$

The rest of parameters for C-C bond in graphite are described in Table 2.

We simply use B, TB, and TA as the three sets of Tersoff-like potential parameters, proposed by Brenner et al. (2002), Oh (2010), and Albe & Moller (1998).

6. Elastic properties

Now we will calculate the coefficients $a_{(ijmn)}$ in the stress-strain relation (64) for three-dimensional crystalline solids with a diamond-like structure, and for two-dimensional crystals with a graphene-like structure. Through these coefficients, the elastic properties of them will be obtained and compared to previous experimental and theoretical results.

6.1 Three-dimensional crystals– diamond, silicon and silicon-carbide

As shown in Fig. 5, diamond, silicon, silicon carbide, or boron nitride is composed of a face-centred cubic array with the centre of each tetrahedron filled by carbon or silicon, and four lattice vectors $\mathbf{E}_{(i)}$ ($i = 1, \dots, 4$) must be introduced to describe their structures. Here we consider cubic types of silicon carbide and boron nitride, not hexagonal types. The primitive lattice vectors in the undeformed diamond-like structure, $\mathbf{E}_{(i)}$, will be deformed into $\mathbf{e}_{(i)}$ ($i = 1, \dots, 4$) by an in-plane homogeneous deformation \mathbf{F} . The deformed lattice vectors $\mathbf{e}_{(1)}$, $\mathbf{e}_{(2)}$, and $\mathbf{e}_{(3)}$ determine the external structure of the deformed unit cell, while $\mathbf{e}_{(4)}$ determines its internal structure.

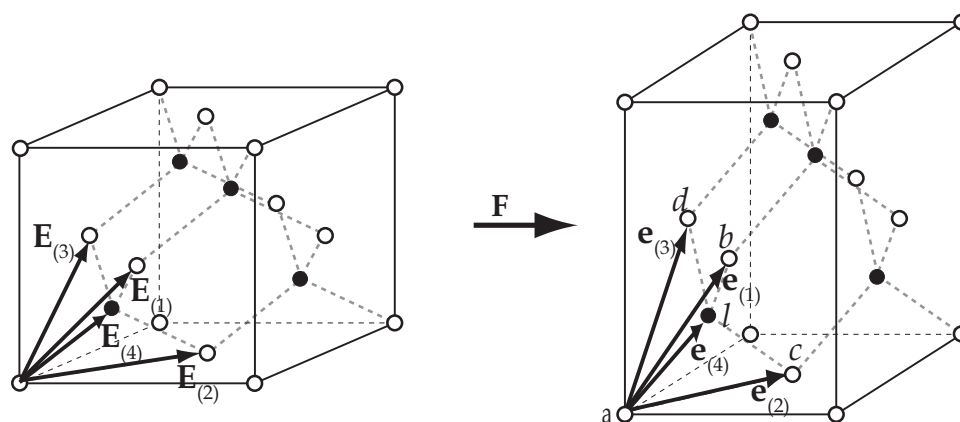


Fig. 5. Schematic of (a) an undeformed diamond-like structure and (b) its deformed structure by a homogeneous deformation \mathbf{F} : diamond (\circ : C atom, \bullet : C atom), silicon (\circ : Si atom, \bullet : Si atom), silicon carbide (\circ : Si atom, \bullet : C atom), or boron nitride (\circ : B atom, \bullet : N atom). The filled circles indicate centre atoms, while the open ones are atoms on each face.

The stress-deformation behaviour of the diamond-like crystals at constant temperature becomes

$$\mathbf{T} = 2\rho\kappa \sum_{m=1}^3 \sum_{n=m}^3 \sum_{i=1}^3 \sum_{j=i}^3 a_{(ijmn)} \mathbf{E}_{(i)} \cdot \boldsymbol{\varepsilon} \mathbf{E}_{(j)} (\mathbf{E}_{(m)} \otimes \mathbf{E}_{(n)} + \mathbf{E}_{(n)} \otimes \mathbf{E}_{(m)}). \quad (77)$$

In view of equation (58) and (66), the coefficient $a_{(ijmn)}$ can be determined by

$$a_{(ijmn)} = \left. \frac{\partial^2 \hat{\Phi}}{\partial I_{(ij)} \partial I_{(mn)}} \right|_{I_{(pq)}=0}, \quad (78)$$

and we require at equilibrium by equations (40) and (66) that

$$\left(\frac{\partial \hat{\Phi}}{\partial I_{(14)}} \right)_{T, I_{(pq) \neq 14}} = \left(\frac{\partial \hat{\Phi}}{\partial I_{(24)}} \right)_{T, I_{(pq) \neq 24}} = \left(\frac{\partial \hat{\Phi}}{\partial I_{(34)}} \right)_{T, I_{(pq) \neq 34}} = 0. \quad (79)$$

	$a_{(1111)}$	$a_{(1122)}$	$a_{(1112)}$	$a_{(1123)}$	$a_{(1212)}$	$a_{(1213)}$
Diamond	1.282	0.146	-0.854	0.281	2.464	-0.378
Silicon	0.124	0.044	-0.083	-0.003	0.160	0.003
Silicon carbide	0.453	0.088	-0.302	0.063	0.745	-0.071
Boron nitride	0.598	0.295	-0.399	-0.096	0.654	0.072

$$\begin{aligned}
 a_{(ijmn)} &= a_{(mnij)}, & a_{(1111)} &= a_{(2222)} = a_{(3333)}, & a_{(1122)} &= a_{(1133)} = a_{(2233)}, \\
 a_{(1112)} &= a_{(1113)} = a_{(2212)} = a_{(2223)} = a_{(3313)} = a_{(3323)}, & a_{(1123)} &= a_{(2213)} = a_{(3312)}, \\
 a_{(1212)} &= a_{(1313)} = a_{(2323)}, & a_{(1213)} &= a_{(1223)} = a_{(1323)}
 \end{aligned}$$

Table 3. The coefficients $a_{(ijmn)}$ of diamond, silicon, and silicon carbide using the Tersoff potential. Here the unit of the coefficient is [eV Å⁻⁴].

The internal lattice vector, $\mathbf{e}_{(4)}$, will be determined by equation (79).

Under the assumption that the deformation shown in Fig. 5 is infinitesimal, all of the distances between two atoms which are not covalently bonded are greater than the cutoff radius for the potentials described in Sect. 5.2. This means that the total stored energy in the diamond-like structure is just the sum of all covalent bond energies:

$$\begin{aligned}
 \hat{\Phi} &= 4(\Phi_{al} + \Phi_{bl} + \Phi_{cl} + \Phi_{dl}) \\
 &= \hat{\Phi} \left(I_{(11)}, I_{(12)}, I_{(13)}, I_{(22)}, I_{(23)}, I_{(33)}, I_{(14)}, I_{(24)}, I_{(34)} \right),
 \end{aligned} \tag{80}$$

because the bond lengths and angles are determined by the invariants.

Using equations (78) and (80), we calculate the coefficients $a_{(ijmn)}$ for diamond, silicon, silicon carbide, and boron nitride and summarize them in Table 3. Here the Tersoff (1988; 1989) potential given in Sect. 5.2.1 is used.

For a cubic elastic material, all of the components of stress can be expressed in terms of strain components using the three independent elastic constants: C_{1111} , C_{1122} , and C_{1212} (Lovett, 1999, p. 66). Thus, the experiments are focusing on determining these three elastic constants with various techniques. These values for the cubic crystals are listed in Table 4 and compared with those calculated by our results, equation (82). In calculating the elastic constants, we express equation (64) in the index notation:

$$\begin{aligned}
 T_{\alpha\beta} &= 2\rho\kappa \sum_{m=1}^3 \sum_{n=m}^3 \sum_{i=1}^3 \sum_{j=i}^3 a_{(ijmn)} E_{(i)\gamma} E_{(j)\delta} (E_{(m)\alpha} E_{(n)\beta} + E_{(n)\alpha} E_{(m)\beta}) \varepsilon_{\gamma\delta} \\
 &\equiv C_{\alpha\beta\delta\gamma} \varepsilon_{\gamma\delta},
 \end{aligned} \tag{81}$$

where

$$C_{\alpha\beta\gamma\delta} = 2\rho\kappa \sum_{m=1}^3 \sum_{n=m}^3 \sum_{i=1}^3 \sum_{j=i}^3 a_{(ijmn)} E_{(i)\delta} E_{(j)\gamma} (E_{(m)\alpha} E_{(n)\beta} + E_{(n)\alpha} E_{(m)\beta}). \tag{82}$$

As seen in Table 4, our theory with the Tersoff potential could well estimate the elastic constants of diamond, silicon, and silicon carbide measured by various experiments: ultrasonic pulse technique (McSkimin & Andreatch, 1972), Brillouin light scattering (Grimsditch & Ramdas, 1975; Lee & Joannopoulos, 1982; Djemia et al., 2004), except for the elastic constants of boron nitride. A Tersoff-like potential, the Tersoff-Albe potential, give a more appropriate set of the elastic constants of boron nitride than the Tersoff potential.

	C_{1111} [GPa]	C_{1122} [GPa]	C_{1212} [GPa]
Diamond	1082	111	646
(exp.) ^f	1079	124	578
Silicon	144	76	69
(exp.) ^g	166	64	79
Silicon carbide	429	117	252
(exp.) ^h	363-395	132-154	149-236
Boron nitride by Tersoff	494	331	177
by Tersoff-Albe	946	131	568
(exp.) ⁱ	820	190	480

^f measured by McSkimin & Andreatch (1972); Grimsditch & Ramdas (1975)

^g measured by McSkimin & Andreatch (1964)

^h measured by Lee & Joannopoulos (1982); Djemia et al. (2004)

ⁱ measured by Grimsditch & Zouboulis (1994)

Table 4. Elastic constants of diamond, silicon, and silicon carbide determined by our theory and measured by experiments.

6.2 Two-dimensional crystals—carbon nanotube and boron nitride nanotube

CNTs and BNNTs including their plane sheets are examples of what we will characterize as two-dimensional crystals. They are two-dimensional in the sense that atoms reside only in a surface or interface between two phases, typically two gases (air), a gas and a solid, or two solids. As illustrated in Fig. 6(a), graphene or BN sheet is composed of a regular two-dimensional array of hexagonal rings of atoms. The nanotubes depicted in Figs. 6(b) and 6(c) have structures of rolled-up sheets and are generally expressed as (m, n) by the method of rolling from the sheets. Here m and n are integers of the chiral vector of the tubes

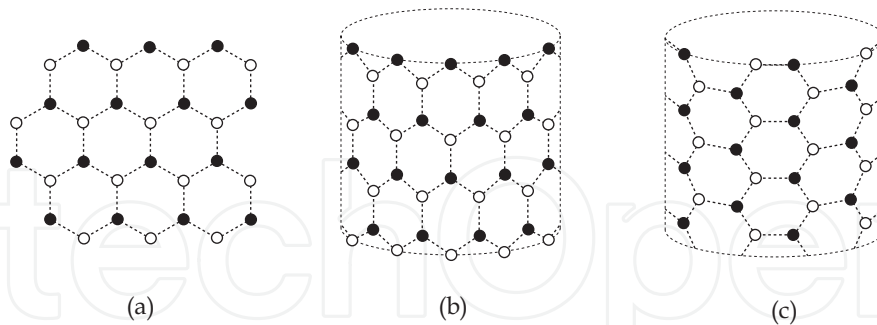


Fig. 6. Structures of two-dimensional crystals: (a) a plane sheet, (b) a zigzag nanotube, and (c) an armchair nanotube: graphene and CNT (○: C atom, ●: C atom), BN sheet or BNNT (○: B atom, ●: N atom) (Oh, 2010).

(Dresselhaus et al., 1995) and uniquely determine the diameter and the chiral angle of the tubes:

$$\text{Diameter} = \frac{[3(m^2 + n^2 + mn)]^{1/2}}{\pi} d_0, \quad \text{Angle} = \arctan \left[\frac{\sqrt{3}n}{2m + n} \right], \quad (83)$$

where d_0 is the bond length. The $(m,0)$ types of tubes are called *zigzag*, while (m,m) types are called *armchair*.

As shown in Fig. 7, the crystal structure deformed by a in-plane small deformation, \mathbf{F} , is determined by both two external lattice vectors, $\mathbf{e}_{(1)}$ and $\mathbf{e}_{(2)}$, and the internal lattice vector, $\mathbf{e}_{(3)}$.

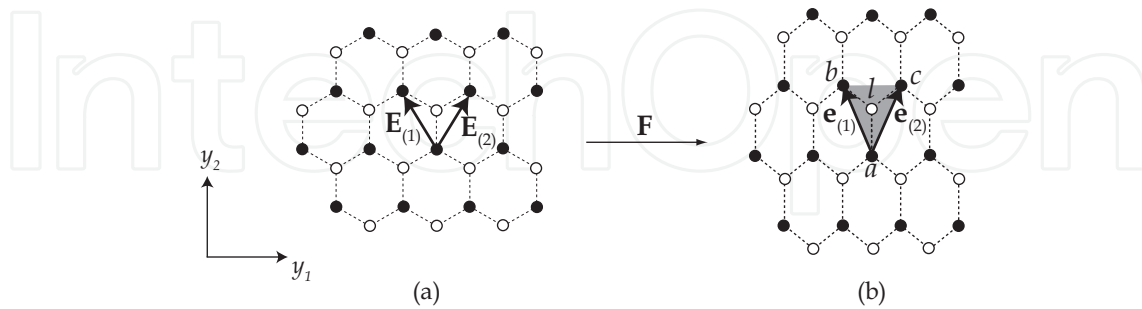


Fig. 7. Primitive lattice vectors (a) in an undeformed plane sheet and (b) in its deformed sheet by an in-plane deformation, \mathbf{F} : graphene (\circ : C atom, \bullet : C atom), BN sheet (\circ : B atom, \bullet : N atom).

In view of equation (11) and (66), the intermolecular potential energy of the two-dimensional crystals at constant temperature is expressed in terms of five invariants:

$$\hat{\Phi} = \hat{\Phi} \left(I_{(11)}, I_{(12)}, I_{(22)}, I_{(13)}, I_{(23)} \right), \tag{84}$$

and the stress-deformation behaviour of the crystals becomes

$$\mathbf{T}^{(\sigma)} = 2\rho_{\kappa}^{(\sigma)} \sum_{m=1}^2 \sum_{n=m}^2 \sum_{i=1}^2 \sum_{j=i}^2 a_{(ijmn)} \mathbf{E}_{(i)} \cdot \boldsymbol{\varepsilon}^{(\sigma)} \mathbf{E}_{(j)} (\mathbf{E}_{(m)} \otimes \mathbf{E}_{(n)} + \mathbf{E}_{(n)} \otimes \mathbf{E}_{(m)}) \tag{85}$$

In addition, we also require at equilibrium by equations (40) and (66) that

$$\left(\frac{\partial \hat{\Phi}}{\partial I_{(13)}} \right)_{T, I_{(pq \neq 13)}} = \left(\frac{\partial \hat{\Phi}}{\partial I_{(23)}} \right)_{T, I_{(pq \neq 23)}} = 0. \tag{86}$$

The internal lattice vector $\mathbf{e}_{(3)}$ will be determined by equation (86).

In a very similar way to the three-dimensional analysis, we can obtain the coefficient $a_{(ijmn)}$ as well as the elastic properties. As mentioned in previous section, all of the distances between two atoms which are not covalently bonded greater than the cutoff radius. Thus the intermolecular potential of the representative triangle lattice a - b - c in Fig. 7(b) is just the sum of three interactions and is also function of the five invariants:

$$\begin{aligned} \hat{\Phi} &= \Phi_{al} + \Phi_{bl} + \Phi_{cl} \\ &= \hat{\Phi} \left(I_{(11)}, I_{(12)}, I_{(22)}, I_{(13)}, I_{(23)} \right) \end{aligned} \tag{87}$$

because the bond lengths and angles are determined by the invariants.

Using equation (78) and the Tersoff-like potential described in Sect. 5.2.2, we calculate the coefficients $a_{(ijmn)}$ for CNT and BNNTs and finally determine their azimuthal and axial

Young's moduli as well as their Poisson's ratios:

$$E_1 = \frac{T_{11}^{(\sigma)}}{\varepsilon_{11}^{(\sigma)}} \Big|_{\varepsilon^{(\sigma)} \rightarrow 0}, \quad E_2 = \frac{T_{22}^{(\sigma)}}{\varepsilon_{22}^{(\sigma)}} \Big|_{\varepsilon^{(\sigma)} \rightarrow 0}, \quad \text{and} \quad \nu_{12} = -\frac{\varepsilon_{11}^{(\sigma)}}{\varepsilon_{22}^{(\sigma)}} \Big|_{\varepsilon \rightarrow 0}, \quad (88)$$

with the help of equation (85).

In calculating the elastic properties we use the interlayer distance of 3.4 Å and 3.3 Å as the wall thicknesses of the CNTs and BNNTs (Krishnan et al., 1998; Salvetat et al., 1999; Yu et al., 2000; Verma et al., 2007). These results are displayed in Fig. 8.

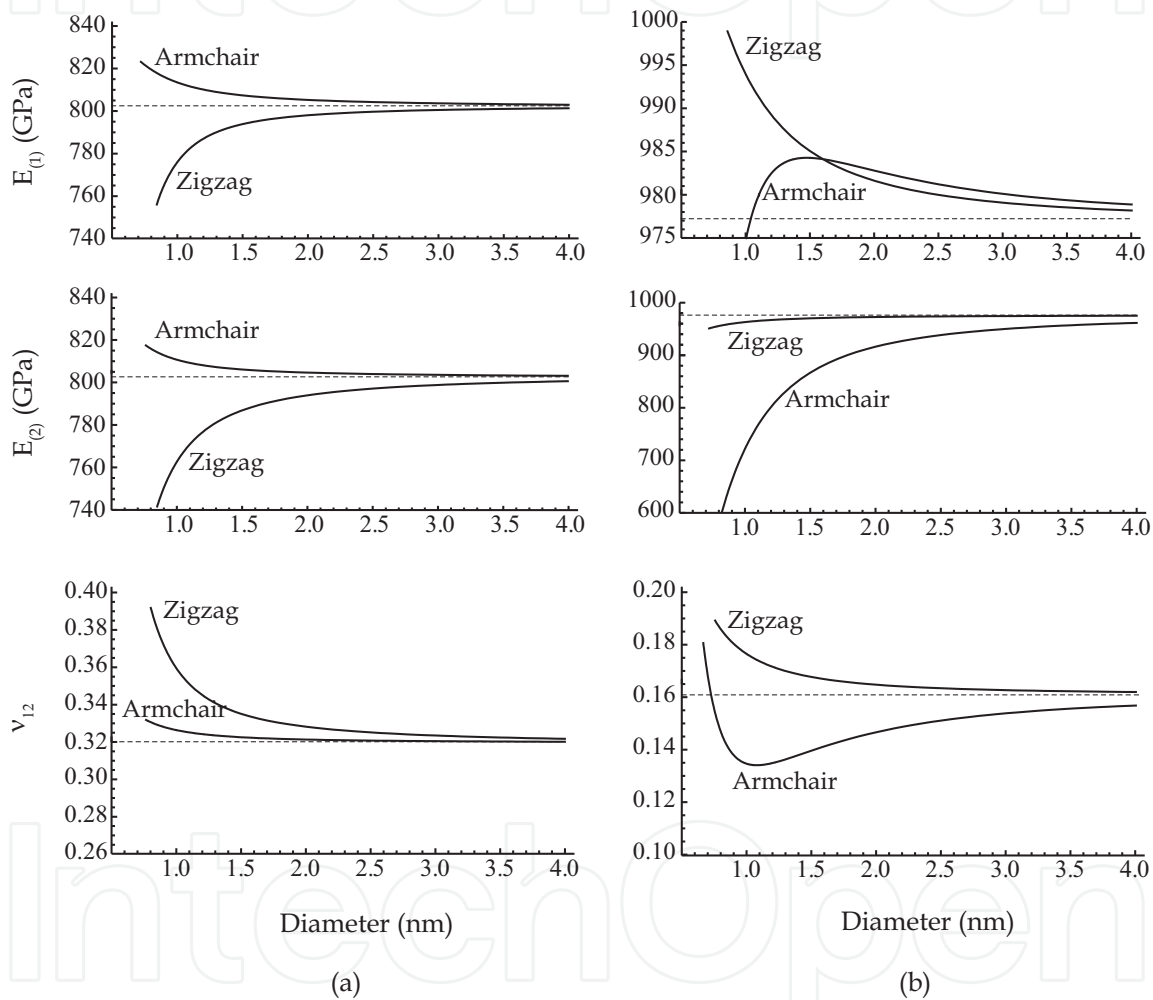


Fig. 8. Young's moduli and Poisson's ratio of (a) CNTs and (b) BNNTs. The dot lines indicate values corresponding to their plane sheets: graphene and BN sheets.

It is clear that the elastic properties of CNTs and BNNTs approach to those of their plane sheets, as the diameter of the nanotube increases. The Young's moduli of graphene and BN sheets are 802.4 and 977.2 GPa, and the Poisson's ratios of graphene and BN sheets are 0.32 and 0.161, respectively. It should be noticed that both azimuthal and axial Young's moduli of the plane sheet have to be the same due to isotropy in the plane of the sheet. While nanotubes are a little deviated from isotropy because of the effect of their curvatures and the anisotropy gradually disappears with decrease in curvature of the nanotubes.

As the diameter increases, both of the Young's moduli of armchair CNTs decrease and ultimately approach to the Young's modulus of the graphene sheet, whereas both of the Young's moduli of zigzag CNTs increase. In the case of BNNTs, the axial Young's moduli, $E_{(2)}$, increase with the diameter of nanotubes. On the contrary, the azimuthal Young's moduli, $E_{(1)}$, of armchair BNNTs show a maximum value at a relatively small diameter and slightly decrease with increase in diameter. A similar phenomenon has been reported for the axial Young moduli of BNNTs (Verma et al., 2007). This may be closely related to the position of the equilibrium point corresponding to the third lattice vector in the deformed configuration, $\mathbf{e}_{(3)}$. As illustrated in Fig. 9, the equilibrium points for the zigzag nanotubes are located below the centroid, which is the equilibrium point for graphene or BN sheet. As the diameter increases, the equilibrium point is getting closed to the centroid. The opposite way happens to be the armchair types of nanotubes.

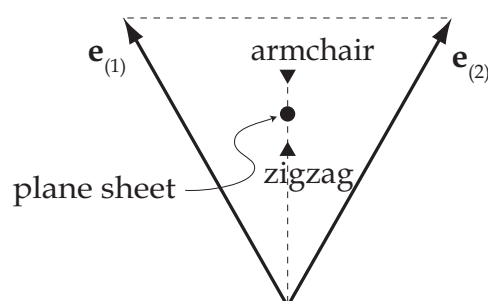


Fig. 9. The equilibrium position in the deformed configuration.

Experimentalists have reported values for only the axial Young's modulus, E_2 . Salvetat et al. (1999) estimated 810 ± 410 GPa of the Young's modulus by measuring the load-deflection of single-walled carbon nanotubes (SWCNTs). From tensile-loading experiments, Yu et al. (2000) measured the Young's modulus of SWCNTs in the range from 320 to 1471 GPa. Our result is also in good agreement with a theoretical result determined by atomistic calculations (Cornwell & Wille, 1997, 800 GPa). Besides, the Young's modulus of 1000 GPa has been reported by some theoretical calculations (Lu, 1997; Popov et al., 1999; Sanchez-Portal et al., 1999).

Using the electric-field-induced resonance method, Suryavanshi et al. (2004) obtained the axial Young's moduli of 18 BNNTs whose diameters are from 34 to 94 nm. The values were irregularly distributed in the range of 550~1031 GPa with an average value of 722 GPa. Chopra & Zettl (1998) have measured the axial Young's modulus from a cantilevered BNNT equipped in transmission electron microscope. It was 1220 ± 240 GPa. The elastic properties of BNNTs have been also theoretically calculated from quantumistic and atomistic simulation methods. Hernández et al. (1999) obtained 862~940 GPa for the axial Young's moduli of BNNTs whose diameters range from 0.8 to 2.1 nm using the tight-binding method. In addition, they showed that the axial Young's moduli of both zigzag and armchair BNNTs increase as the diameter of the nanotubes increases. It corresponds to our results shown in Fig. 8. The Poisson's ratio of the BNNTs was from 0.232 to 0.268. Verma et al. (2007) have also calculated the axial Young's moduli and the Poisson's ratios of zigzag and armchair BNNTs: 982~1110.6 GPa, 0.13~0.16. These Poisson's ratios are close to our result as depicted in Fig. 8.

Consequently, the elastic properties of two-dimensional crystals obtained from the Tersoff-like potentials are in very good agreement with both experimental and theoretical ones.

7. References

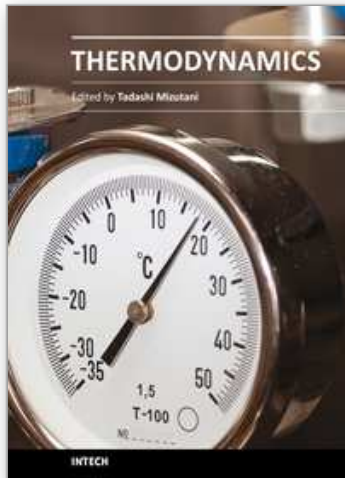
- Albe, K. & Möller, W. (1998). Modelling of boron nitride: Atomic scale simulations on thin film growth. *Comput. Mater. Sci.*, Vol. 10, 111-115.
- Brenner, D. W. (1990). Empirical potential for hydrocarbons for use in simulation the chemical vapor deposition of diamond films. *Phys. Rev. B*, Vol. 42, 9458-9471.
- Brenner, D. W.; Shenderova, O. A.; Harrison, J. A.; Stuart, S. J.; Ni, B. & Sinnott, S. B. (2002). A second-generation reactive empirical bond order (REBO) potential energy expression for hydrocarbons. *J. Phys.: Condens. Matter*, Vol. 14, 783-802.
- Chopra, N. G. & Zettl, A. (1998). Measurement of the elastic modulus of a multi-wall boron nitride nanotube. *Solid State Commun.*, Vol. 105, 297-300.
- Cornwell, C. F. & Wille, L. T. (1997). Elastic properties of single-walled carbon nanotubes in compression. *Solid State Commun.*, Vol. 101, 555-558.
- Djemia, P.; Roussigne, Y.; Dirras, G. F. & Jackson, K. M. (2004). Elastic properties of β -SiC films by Brillouin light scattering. *J. Appl. Phys.*, Vol. 95, 2324-2340.
- Dresselhaus, M. S.; Dresselhaus, G. & Saito, R. (1995). Physics of carbon nanotubes. *Carbon*, Vol. 33, 883-891.
- Edelen, D. G. B. (1975). The thermodynamics of evolving chemical systems and their approach to equilibrium. *Adv. Chem. Phys.*, Vol. 33, 399-422.
- Ericksen, J. L. (1992). Bifurcation and martensitic transformations in Bravais lattices. *J. Elasticity*, Vol. 28, 55-78, ISSN
- Grimsditch, M. H. & Ramdas, A. K. (1975). Brillouin scattering in diamond. *Phys. Rev. B*, Vol. 11, 3139-3148.
- Grimsditch, M. H. & Zouboulis, E. S. (1994). Elastic constants of boron nitride. *J. Appl. Phys.*, Vol. 76, 832-834.
- Hernández, E.; Goze, C.; Bernier, P. & Rubio, A. (1999). Elastic properties of single-wall nanotubes. *Appl. Phys. A*, Vol. 68, 287-292.
- James, R. D. & Hane, K. F. (2000). Martensitic transformations and shape memory materials. *Acta Mater.*, Vol. 48, 197-222.
- Klein, P. M. (1996). *A Virtual Internal Bond Approach to Modeling Crack Nucleation and Growth*, Stanford University, Ph. D. thesis.
- Koga, H.; Nakamura, Y.; Watanabe, S. & Yoshida, T. (2001). Molecular dynamics study of deposition mechanism of cubic boron nitride. *Sci. Technol. Adv. Mater.*, Vol. 2, 349-356.
- Krishnan, A.; Dujardin, E.; Ebbesen, T. W.; Yianilos, P. N. & Treacy, M. M. J. (1999). Young's modulus of single-walled nanotubes. *Phys. Rev. B*, Vol. 58, 14013-14019.
- Kroll, P. M. (1996). *Computer Simulations and X-ray Absorption Near Edge Structure of Silicon Nitride and Silicon Carbonitride*, Technische Hochschule Darmstadt, Ph. D. thesis, Darmstadt, Germany.
- Lee, D. H. & Joannopoulos, J. D. (1982). Simple Scheme for Deriving Atomic Force Constants: Application to SiC. *Phys. Rev. Lett.*, Vol. 48, 1846-1849.
- Lovett, D. R. (1999). *Tensor Properties of Crystals*, Taylor & Francis, Second ed., ISBN 0-750-306262, Bristol and Philadelphia.
- Lu, J. P. (1997). Elastic properties of carbon nanotubes and nanoropes. *Phys. Rev. Lett.*, Vol. 79, 1297-1300.
- Matsunaga, K.; Fisher, C. & Matsubara, H. (2000). Tersoff potential parameters for simulating cubic boron carbonitrides. *Jpn. J. Appl. Phys.*, Vol. 39, L48-L51.
- McSkimin, H. J. & Andreatch, P. (1964). Elastic moduli of silicon vs hydrostatic pressure at 25°C and -195.8°C. *J. Appl. Phys.*, Vol. 35, 2161-2165.

- McSkimin, H. J. & Andreatch, P. (1972). Elastic Moduli of Diamond as a Function of Pressure and Temperature. *J. Appl. Phys.*, Vol. 43, 2944-2948.
- Moon, W. H. & Hwang, H. J. (2004). Molecular-dynamics simulation of structure and thermal behaviour of boron nitride nanotubes. *Nanotechnology*, Vol. 15, 431-434.
- Oh, E.-S. (2010). Elastic properties of boron-nitride nanotubes through the continuum lattice approach. *Mater. Lett.*, Vol. 64, 869-862.
- Oh, E.-S.; Slattery, J. C. & Lagoudas, D. C. (2005). Thermodynamics of two-dimensional single-component elastic crystalline solids: single-wall carbon nanotubes. *Phil. Mag.*, Vol. 85, No. 20, 2249-2280.
- Oh, E.-S. & Slattery, J. C. (2008). Nanoscale thermodynamics of multicomponent, elastic, crystalline solids: diamond, silicon, and silicon carbide. *Phil. Mag.*, Vol. 88, No. 3, 427-440.
- Popov, V. N.; Van Doren, V. E. & Balkanski, M. (1999). Lattice dynamics of single-walled carbon nanotubes. *Phys. Rev. B*, Vol. 59, 8355-8358.
- Salvetat, J. P.; Briggs, G. A. D.; Bonard, J. M.; Bacsá, R. R.; Kulik, A. J.; Stockli, T.; Burnham, N. A. & Forro, L. (1999). Elastic and shear moduli of single-walled carbon nanotube ropes. *Phys. Rev. Lett.*, Vol. 82, No. 3, 944-947.
- Sanchez-Portal, D.; Artacho, E.; Solar, J. M.; Rubio, A. & Ordejon, P. (1999). Ab initio structural, elastic, and vibrational properties of carbon nanotubes. *Phys. Rev. B*, Vol. 59, 12678-12688.
- Slattery, J. C. (1999). *Advanced Transport Phenomena*, Cambridge University Press, ISBN 0-521-63203X, Cambridge.
- Slattery, J. C. & Lagoudas, D. C. (2005). Thermodynamics of multicomponent, elastic crystalline solids. *Mech. Mater.*, Vol. 37, 121-141.
- Slattery, J. C.; Sagis, L. M. C. & Oh, E.-S. (2007). *Interfacial Transport Phenomena*, Springer, Second ed., ISBN 0-387-38438-3, New York.
- Suryavanshi, A. P.; Yu, M. F.; Wen, J.; Tang, C. & Bando, Y. (2004). Elastic modulus and resonance behavior of boron nitride nanotubes. *Appl. Phys. Lett.*, Vol. 84, 2527-2529.
- Tersoff, J. (1988). New empirical approach for the structure and energy of covalent systems. *Phys. Rev. B*, Vol. 37, 6991-7000.
- Tersoff, J. (1989). Modeling solid-state chemistry: Interatomic potentials for multicomponent systems. *Phys. Rev. B*, Vol. 39, 5566-5568.
- Tester, J. W. & Modell, M. (1996). *Thermodynamics and Its Applications*, Prentice Hall, Third ed., ISBN 0-139-15356X, New Jersey.
- Truesdell, C. & Noll, W. (1965). The non-linear field theories of mechanics, In: *Handbuch der Physik*, Flügge, S. (Ed.), 1-602, Springer-Verlag, ISBN, Berlin.
- Verma, V.; Jindal, V. K. & Dharamvir, K. (2007). Elastic moduli of a boron nitride nanotube. *Nanotechnology*, Vol. 18, 435711.
- Yin, M. T. & Cohen, M. L. (1983). Structural theory of graphite and graphitic silicon. *Phys. Rev. B*, Vol. 29, 6996-6998.
- Yin, M. T. & Cohen, M. L. (1983). Will Diamond Transform under Megabar Pressures?. *Phys. Rev. Lett.*, Vol. 50, 2006-2009.
- Yu, M. F.; Lourie, O.; Dyer, M. J.; Moloni, K.; Kelly, T. F. & Ruoff, R. S. (2000). Strength and breaking mechanism of multiwalled carbon nanotubes under tensile load. *Science*, Vol. 287, 637-640.
- Zanzotto, G. (1992). On the material symmetry group of elastic crystals and the Born rule. *Arch. Rational Mech. Anal.*, Vol. 121, 1-36.

Zhang, P. ; Huang, Y.; Geubelle, P. H.; Klein, P. A. & Hwang, K. C. (2002). The Elastic Modulus of Single-Wall Carbon Nanotubes: A Continuum Analysis Incorporating Interatomic Potentials. *Int. J. Solids Struct.*, Vol. 39, 3893-3906.

IntechOpen

IntechOpen



Thermodynamics

Edited by Prof. Mizutani Tadashi

ISBN 978-953-307-544-0

Hard cover, 440 pages

Publisher InTech

Published online 14, January, 2011

Published in print edition January, 2011

Progress of thermodynamics has been stimulated by the findings of a variety of fields of science and technology. The principles of thermodynamics are so general that the application is widespread to such fields as solid state physics, chemistry, biology, astronomical science, materials science, and chemical engineering. The contents of this book should be of help to many scientists and engineers.

How to reference

In order to correctly reference this scholarly work, feel free to copy and paste the following:

Eun-Suok Oh (2011). Application of the Continuum-Lattice Thermodynamics, Thermodynamics, Prof. Mizutani Tadashi (Ed.), ISBN: 978-953-307-544-0, InTech, Available from:

<http://www.intechopen.com/books/thermodynamics/application-of-the-continuum-lattice-thermodynamics>

INTECH

open science | open minds

InTech Europe

University Campus STeP Ri
Slavka Krautzeka 83/A
51000 Rijeka, Croatia
Phone: +385 (51) 770 447
Fax: +385 (51) 686 166
www.intechopen.com

InTech China

Unit 405, Office Block, Hotel Equatorial Shanghai
No.65, Yan An Road (West), Shanghai, 200040, China
中国上海市延安西路65号上海国际贵都大饭店办公楼405单元
Phone: +86-21-62489820
Fax: +86-21-62489821

© 2011 The Author(s). Licensee IntechOpen. This chapter is distributed under the terms of the [Creative Commons Attribution-NonCommercial-ShareAlike-3.0 License](#), which permits use, distribution and reproduction for non-commercial purposes, provided the original is properly cited and derivative works building on this content are distributed under the same license.

IntechOpen

IntechOpen